

Towards Understanding the Adversarial Vulnerability of Skeleton-based Action Recognition

Tianhang Zheng, Sheng Liu, Changyou Chen, Junsong Yuan, Baochun Li, Kui Ren
State University of New York at Buffalo, University of Toronto, Zhejiang University

ABSTRACT

Skeleton-based action recognition has attracted increasing attention due to its strong adaptability to dynamic circumstances and potential for broad applications such as autonomous and anonymous surveillance. With the help of deep learning techniques, it has also witnessed substantial progress and currently achieved around 90% accuracy in benign environment. On the other hand, research on the vulnerability of skeleton-based action recognition under different adversarial settings remains scant, which may raise security concerns about deploying such techniques into real-world systems. However, filling this research gap is challenging due to the unique physical constraints of skeletons and human actions. In this paper, we attempt to conduct a thorough study towards understanding the adversarial vulnerability of skeleton-based action recognition. We first formulate generation of adversarial skeleton actions as a constrained optimization problem by representing or approximating the physiological and physical constraints with mathematical formulations. Since the primal optimization problem with equality constraints is intractable, we propose to solve it by optimizing its unconstrained dual problem using ADMM. We then specify an efficient plug-in defense, inspired by recent theories and empirical observations, against the adversarial skeleton actions. Extensive evaluations demonstrate the effectiveness of the attack and defense method under different settings.

1 INTRODUCTION

Action recognition is an important task in computer vision, motivated by many downstream applications such as video surveillance and indexing, and human-machine interaction [6]. It is also a very challenging task since it requires to capture long-term spatial-temporal context and understand the semantics of actions. One method proposed by the community is to learn action recognition on the human skeleton information collected by cameras or sensors, where an action is represented by a time series of human joint locations. Compared with video streams, skeleton representation is more robust to the variance of background conditions, and also easier-to-handle for machine learning models due to its compact representation. Recent advances in deep learning techniques boost the performance of this method. Currently, a variety of deep learning model structures have been applied to skeleton-based action recognition, including convolutional neural networks [15, 20], recurrent neural networks [21, 30], and graph neural networks [23, 29, 37]. On the other hand, existing work has demonstrated the vulnerability of deep learning techniques to adversarial examples in many application domains. This phenomenon gives us a good reason to suspect that the DNNs for skeleton-based action recognition might also be vulnerable to adversarial skeleton examples despite achieving high accuracy in a benign environment. Note that a thorough study on the adversarial vulnerability of action-recognition

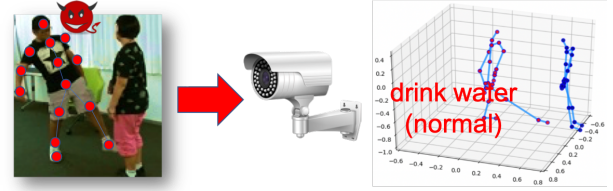


Figure 1: The targeted Setting: misleading the model to recognize “kicking people” as “drinking water” (normal action) by perturbing the skeleton action. To launch the attack in a real-world scenario (e.g., under a surveillance camera), the adversarial skeleton action should satisfy certain constraints. The figure is drawn based on [28].

models is indispensable before deploying them to real-world applications such as surveillance systems because otherwise, the potential adversaries might easily deceive those systems by generating and imitating specific adversarial actions. However, the study on the adversarial skeleton examples is scant and non-trivial*, due to the fundamental differences between the properties of adversarial skeleton actions and other adversarial examples. The differences are mainly caused by the bones between joints and the joint angles, which impose unique spatial constraints on skeleton data [28]. Specifically, in the generated adversarial skeleton actions, lengths of the bones must be maintained the same, and joint angles can not violate certain physiological structures. Otherwise, the adversarial actions are not reproducible by the individuals who perform the original actions. Also, considering the physical conditions of human beings, the speeds of motions in the adversarial actions should also be constrained.

To address the above issues, in this paper, we propose an optimization based method for generating adversarial skeleton actions. Specifically, we formulate the generation of adversarial skeleton actions as a constrained optimization problem by representing those constraints with mathematical equations. Since the primal constrained problem is intractable, we turn to solve its dual problem. Moreover, since all the constraints are represented by mathematical equations, both primal and dual variables are nonrestrictive in the dual problem. We further specify an efficient algorithm based on ADMM to solve the unconstrained dual problem, in which the internal minimization objective is optimized by an Adam optimizer, and the external maximization objective is optimized by one-step gradient ascent. We show that this algorithm can find an adversarial skeleton action within 200 internal steps.

Other than the attack, we further propose an efficient defense against adversarial skeleton actions based on previous theories and empirical observations. Our defense consists of two core steps, *i.e.*,

*The only parallel work is detailed in section 2.3.

adding Gaussian noise and Gaussian filtering to action data. The first step, adding Gaussian noise, is inspired by the recent advance in certified defenses. Specifically, adding Gaussian noise to the input is proved to be a certified defense, which means additive Gaussian noise on the adversarial examples can guarantee the model to output a correct prediction (with high probability), as long as the adversarial perturbation is restricted within a certain radius in the neighbor of the original data sample. Note that there are also several other methods to certify model robustness, such as dual approach, interval analysis and abstract interpretations [8, 12, 26, 33, 35]. We adopt the Gaussian noise method because it is simple, effective, and more importantly, scalable to complicated models. Note that skeleton-based action recognition models are always more complicated than the common ConvNets certified by [8, 12, 26, 33, 35]. The second step is to smooth the skeleton frames along the temporal axis using a Gaussian filter. This step will not affect the robustness certified by the first step according to the post-processing property [7, 18, 20], but can always filter out a certain amount of adversarial perturbation and random noise in practice, thus making our defense applicable to normally trained models.

Our proposed attack and defense are evaluated on two open-source models, *i.e.*, 2s-AGCN and HCN[†]. Extensive evaluations show that our attack can achieve 100% attack success rate with almost no violation of the constraints. Moreover, the visualization results, including images and videos, demonstrate that the difference between the original and adversarial skeleton actions is imperceptible. Extensive evaluations also show that our defense is effective and efficient. Specifically, our defense can improve the empirical accuracy of normally trained models to over 60% against adversarial skeleton actions under different settings.

To summarize, our main contribution is four-fold:

- (1) We identify the constraints needed to be considered in adversarial skeleton actions, and formulate the problem of generating adversarial skeleton actions as a constrained optimization problem by representing those constraints as mathematical equations.
- (2) We propose to solve the primal constrained problem by optimizing the dual problem using ADMM, which is the first trial on generating adversarial actions with ADMM and yields outstanding performance.
- (3) We propose an efficient two-step plug-in defense against adversarial skeleton actions, and specify the defense in both inference and certification stages.
- (4) We conduct extensive evaluations, and provide several interesting observations regarding adversarial skeleton actions based on the experimental results.

2 PRELIMINARIES

2.1 Definitions and Notations

Let \mathbf{x} and $l \in \{1, 2, \dots, L\}$ respectively denote a data sample and the label, where L is the number of all possible classes. For an image, \mathbf{x} is a 2D matrix. For a skeleton action studied in this paper, $\mathbf{x} \triangleq \{(x_i^\tau, y_i^\tau, z_i^\tau)_{i=1}^I\}_{\tau=1}^T$, where $(x_i^\tau, y_i^\tau, z_i^\tau)$ denotes the position

[†]We select these two models because the authors have released the code and hyperparameters on Github so that we can correctly reproduce the results. Also, these two models achieve fairly good performance.

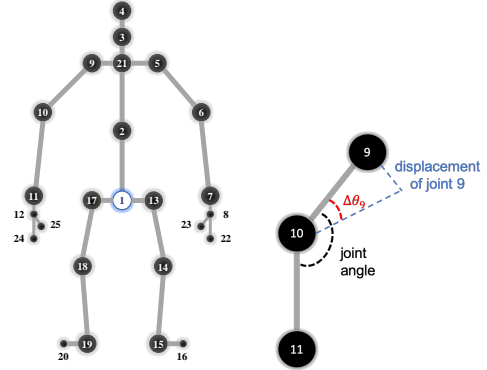


Figure 2: Skeleton Representation

(coordinates) of the i -th joint of the τ -th skeleton frame in an action sequence, with I and T denoting the number of joints in a skeleton and the number of skeleton frames in an action sequence, respectively. The corresponding adversarial skeleton action is denoted by $\mathbf{x}' \triangleq \{(x_i'^\tau, y_i'^\tau, z_i'^\tau)_{i=1}^I\}_{\tau=1}^T$. We take the skeletons in the largest dataset, *i.e.*, NTU RGB+D dataset, as an example. As shown in figure 2, in a skeleton, there are totally 25 joints in a skeleton frame, and thus $I = 25$. The number of frames T differs for each skeleton action, and usually, we subsample a constant number of frames from each sequence or pad zeros after each sequence to endow all the skeleton actions with the same T . Let $\mathbf{F}_\Theta(\cdot)$ denote a classification network, where Θ represents the network weights. The logit output on \mathbf{x} is denoted by $\mathbf{F}_\Theta(\mathbf{x})$ with L elements ($\{\mathbf{F}_{\Theta,k}(\mathbf{x}) \mid k = 1, \dots, L\}$). $\mathbf{F}_\Theta(\cdot)$ can correctly classify \mathbf{x} iff $\arg\max_k \mathbf{F}_{\Theta,k}(\mathbf{x}) = l$. The goal of adversarial attacks is to find an adversarial sample \mathbf{x}' , which satisfies several pre-defined constraints, such that $\arg\max_k \mathbf{F}_{\Theta,k}(\mathbf{x}') \neq l$ or $\arg\max_k \mathbf{F}_{\Theta,k}(\mathbf{x}) = l_t$ (l_t is the target label). A commonly-used constraint is that \mathbf{x}' should be close to the original sample \mathbf{x} according to some distance metric.

2.2 DNNs for Skeleton-based Action Recognition

In the following, we briefly introduce the two DNNs used for evaluation of our proposed attack method in this project. HCN is a CNN-based end-to-end hierarchical network for learning global co-occurrence features from skeleton data [20]. HCN is designed to learn different levels of features from both raw skeleton and skeleton motion. The joint-level features are learned by a multi-layer CNN, and the global co-occurrence features are learned from the fused joint-level features. At the end, the co-occurrence features are also fed to a fully-connected network for action classification. 2s-AGCN is one of the state-of-the-art GCN-based models for skeleton-based action recognition. In contrast to the earliest GCN-based model, (*i.e.*, ST-GCN), 2s-AGCN learns the appropriate graph topology of every skeleton action rather than predefine the graph topology. This enables 2s-AGCN to capture the implicit connections between joints in certain actions, such as the connection between hand and face in the “wiping face” action. Besides, 2s-AGCN also adopts the two-stream framework to learn from both static and

motion information. Overall, 2s-AGCN significantly improves the accuracy of ST-GCN by nearly 7%.

2.3 Adversarial Attacks

After the discovery of adversarial examples, the community has developed hundreds of attack methods to generate adversarial samples. In the following, we mainly introduce four attack methods plus a parallel work, with a discussion on the difference between our proposed method and these attacks.

Fast Gradient Sign Method (FGSM). FGSM is a typical one-step adversarial attack algorithm proposed by [10]. The algorithm updates a benign sample along the direction of the gradient of the loss w.r.t. the sample. Formally, FGSM follows the update rule as

$$\mathbf{x}' = \text{clip}_{[v_{min}, v_{max}]} \{ \mathbf{x} + \epsilon \cdot \text{sign}(\nabla_{\mathbf{x}} \mathcal{L}(\Theta, \mathbf{x}, l)) \}, \quad (1)$$

where ϵ controls the maximum ℓ_{∞} perturbation of the adversarial samples; $[v_{min}, v_{max}]$ is the valid element-wise value range and $\text{clip}_{[a, b]}(\cdot)$ function clips its input into the range of $[a, b]$.

Projected Gradient Descent (PGD). PGD [16, 24] is a strong iterative version of FGSM, which executes Eq. 2.3 for multiple steps with a smaller step size and then projects the updated adversarial examples into the pre-defined ℓ_p -norm ball. Specifically, in each step, PGD updates the sample by

$$\mathbf{x}'_{t+1} = \text{Proj} \{ \mathbf{x}'_t + \alpha \cdot \text{sign}(\nabla_{\mathbf{x}'_t} \mathcal{L}(\Theta, \mathbf{x}'_t, l)) \} \quad (2)$$

The *Proj* function is a clip function for ℓ_{∞} -norm balls, and an ℓ_2 normalizer for ℓ_{∞} -norm balls.

Carlini and Wagner Attack. [5] proposes an attack called C&W attack, which generates ℓ_p -norm adversarial samples by optimization over the C&W loss:

$$\min_{\mathbf{x}'} D(\mathbf{x}, \mathbf{x}') + c \cdot \text{loss}(\mathbf{x}') . \quad (3)$$

In the C&W loss, $D(\mathbf{x}, \mathbf{x}')$ represents some distance metric between the benign sample \mathbf{x} and the adversarial sample \mathbf{x}' , and the metrics used in [5] include ℓ_{∞} , ℓ_0 , and ℓ_2 distances. $\text{loss}(\cdot)$ is a customized loss. It is worth noting that our proposed attack is completely different from PGD or C&W attack. For PGD, C&W, or many other attacks, the simple constraints on the pixel value can be resolved by projection functions or naturally incorporated into the objective by *sigmoid/tanh* function. However, in our scenario, the constrained optimization problem is much more complicated, and thus has to be solved by more advanced methods.

ADMM-based Adversarial Attack. [40] also proposes a framework based on ADMM to generate ℓ_p adversarial examples. However, we note that our proposed attack is also completely different from [40] in two aspects: First, the constraints we consider are more complicated than the ℓ_p -norm constraints, which makes ADMM more appropriate than the other attack algorithms here. Second, we formulate the problem in a completely different manner from [40]. [40] follows the ADMM framework to break the problem defined like Eq. 3 into two sub-problems, while our attack formulates a completely different problem with indispensable equality constraints, and ADMM is naturally an appropriate solution to this problem.

Adversarial Attack on Skeleton Action. Note that [22] is a parallel work that proposes an attack based on FGSM and BIM (PGD) to generate adversarial skeleton actions. Specifically, [22] adapts the FGSM and BIM to skeleton-based action recognition by using a clipping function and an alignment operation to impose the bone and joint constraints on the updated adversarial skeleton actions in each iteration. *However, the method is very different from our work.* First, the joint constraint considered in [22] is not the constraint for joint angles mentioned before. Second, the alignment operation might corrupt the perturbation learned in each iteration. In contrast to [22], we attempt to formulate adversarial skeleton action generation as a constrained optimization problem with equality constraints. Reformulating the equality constraints by Lagrangian multipliers yields an unconstrained dual optimization problem, which does not need any complicated additional operation in the optimization process. Third, we propose to solve the dual optimization problem by ADMM, which is a more appropriate algorithm to optimize complicated constrained problems. Therefore, the attack achieves better performance than [22], which will be detailed in section 6.1. Finally, we specify a defense method against adversarial skeleton actions based on the state-of-the-art theories and our observations.

2.4 Alternating Direction Method of Multipliers (ADMM)

Alternating Direction Method of Multipliers (ADMM) is a powerful optimization algorithm to handle large-scale statistical tasks in diverse application domains. It blends the decomposability of dual ascent with the great convergence property of the method of multipliers. Currently, ADMM plays a significant role in solving statistical problems, such as support vector machines [9], trace norm regularized least squares minimization [38], and constrained sparse regression [3]. Except for convex problems, ADMM is also a widely used solution to some nonconvex problems, whose objective function could be nonconvex, nonsmooth, or both. [34] shows that ADMM is able to converge as long as the objective has a smooth part, while the remaining part can be coupled or nonconvex, or include separable nonsmooth functions. Applications of ADMM to nonconvex problems include network reference [25], global conformal mapping [17], noisy color image restoration [17].

2.5 Adversarial Defenses

Both learning and security communities have developed many defensive methods against adversarial examples. Among them, adversarial training and several certified defenses attract the most attention due to their outstanding/guaranteed performance against strong attacks [2, 13, 32]. In the following, we briefly introduce adversarial training and several certified defenses, including the randomized smoothing method adopted in this paper.

Adversarial Training. Adversarial training is one of the most successful empirical defenses in the past few years [10, 24, 39]. The intuition of adversarial training is to improve model robustness by training the model with adversarial examples. Although adversarial training achieves tremendous success against many strong attacks [1, 31, 41], its performance is not theoretically guaranteed and thus might be compromised in the future. Besides, adversarial training

always requires much more computational resource than standard training, making it not scalable to complicated models.

Certified Defenses. A defense with a theoretical guarantee on its defensive performance is considered as a certified defense. In general, there are three main approaches to design certified defenses. The first approach is to formulate the certification problem as an optimization problem and bound it by dual approach and convex relaxations [8, 27, 35]. The second approach approximates a convex set that contains all the possible outputs of each layer to certify an upper bound on the range of the final output [12, 26, 33]. The third is the randomized smoothing method used in this paper. The only essential operation for this method is to add Gaussian/Laplace noise to the inputs, which is simple and applicable to any deep learning models. [18] first proves that randomized smoothing is a certified defense by theories on differential privacy. [19] improves the certified bound using a lemma on Renyi divergence. Cohen et al. [7] proves a tight bound on the ℓ_2 robust radius certified by adding Gaussian noise using the Neyman-Pearson lemma. [14] further extends the approach of [7] to the *top-k* classification setting. Since the bound proved by [7] is the tightest, the method in [7] is used for certification. In this paper we adopt the approach in [18] due to its ability for efficient inference in practice.

3 THREAT MODEL

3.1 Adversary Knowledge: White-box Setting

In this paper, we follow the white-box setting, where the adversary has full access to the model architecture and parameters. We make this assumption because (i) it is always a safe, conservative, and realistic assumption since we might never know the knowledge of potential adversaries about the model [5], which varies among different adversaries and also changes over time. (ii) For systems/devices equipped with an action recognition model, recognition is more likely to be done locally, or on a local cloud, making the adversary easily acquire the model parameters with his own system/device. Note that although most of the experiments on the proposed attack and defense are done under the white-box setting, we also have several experiments on evaluating the transferability of our attack.

3.2 Adversary Goal: Targeted & Untargeted label Setting

Under the targeted setting, the goal of an adversary is to mislead the recognition model to predict the adversarial skeleton action as a targeted label pre-defined by the adversary. For instance, suppose the adversary is "kicking" someone under a surveillance camera equipped with an action recognition model. It may launch a targeted attack to mislead the model to recognize this violent action as a normal one such as "drinking water". Under the untargeted label settings, an adversary only aims to disable the recognition and thus is considered successful as long as the model makes wrong predictions instead of a specific targeted prediction. In this paper, we propose two objectives suitable for the above two settings respectively, which will be detailed in section 4.4.

3.3 Imperceptibility & Reproducibility

Except for the aforementioned adversary goals, the adversary also requires the adversarial perturbation to be both imperceptible and reproducible. Here "imperceptibility" means it should be difficult for human vision to figure out the adversarial perturbation, *i.e.*, the difference between the original and adversarial skeleton actions. This is not only a common requirement in the previous attacks, but also a useful one in our scenario. Note that it is natural to schedule a periodical examination for an autonomous surveillance system by human labor to check if the system works well. If the system has been fooled by a seemingly "normal" adversarial skeleton action, the mistake might be due to the system itself rather than the adversary who performs the adversarial skeleton action in the examination process. Here "reproducibility" is an additional requirement specific to our scenario. As mentioned in the introduction, *the adversarial skeleton action could be a real threat when it can be reproduced under a real-world system*. Thus, to make our attack a real-world threat, the generated adversarial skeleton actions should satisfy three concrete constraints to be reproducible, which will be detailed in section 4.

4 ADVERSARIAL SKELETON ACTION

In this section, we present our proposed attack, *i.e.*, ADMM attack. We first introduce how to formulate the three constraints into mathematical equations. Then we formulate the constrained optimization problem to generate adversarial skeleton actions under both targeted and untargeted settings. Finally, we elaborate on how to solve the optimization problem by ADMM.

4.1 Bone Constraints

We again take the skeletons in the NTU RGB+D dataset as an example. As shown in Fig. 2, in a skeleton, there are totally 25 joints, forming a total of 24 bones. While the bones are not explicitly considered in modeling, they are strictly connecting to the 25 joints, thus imposing 24 bone-length constraints, *i.e.*, the distance between the joints at the two ends of a bone should remain the same in adversarial skeleton actions. To mathematically represent the 24 bones, we associate each joint with its preceding joint, forming the two ends of a bone. As a result, the 24 preceding-joints for joint-2~joint-25 are denoted as $\mathcal{P} \triangleq \{(x_{p_i}^\tau, y_{p_i}^\tau, z_{p_i}^\tau)_{i=2}^{25}\}$. The corresponding joint indices of the elements in \mathcal{P} are $\{1, 21, 3, 21, 5, 6, 7, 21, 9, 10, 11, 1, 13, 14, 15, 1, 17, 18, 19, 2, 8, 8, 12, 12\}$. We define the i -th bone's length as $B_i^\tau \triangleq \sqrt{(x_i^\tau - x_{p_i}^\tau)^2 + (y_i^\tau - y_{p_i}^\tau)^2 + (z_i^\tau - z_{p_i}^\tau)^2}$. In this regard, the bone constraints can be represented as $L_i^\tau = L_i'^\tau$. Due to the measurement errors in the NTU dataset itself, here we also tolerate very small difference between L_i^τ and $L_i'^\tau$. Therefore, we can finally formulate the bone constraints as

$$|B_i'^\tau - B_i^\tau|/B_i^\tau \leq \epsilon_L, \quad (4)$$

where ϵ_L is usually set as 0.01 ~ 0.03. *Note that inequality constraints in the primal problem will impose inequality constraints on the corresponding Lagrangian variables in the dual problem.* In order to avoid this in the dual problem, we reformulate the above inequality constraints as mathematical equations, *i.e.*, (4) is equivalent to

$$\max\{|B_i'^\tau - B_i^\tau|/B_i^\tau - \epsilon_L, 0\} = 0. \quad (5)$$

4.2 Joint Angle Constraints

Except for the bone-length constraints, we also need to impose constraints on the rotations of the joint angles according to the physiological structures of human beings. Let us also use the NTU dataset as an example. Each joint angle corresponds to the angle between two bones, and thus can be represented by the three joint locations of those two corresponding bones as illustrated in the right of Fig. 2. Note that a natural way to compute the joint angle as shown in Fig. 2 is to first compute the cosine value and then input the value into the arccos function. However, the gradient of arccos function is likely exploded, causing large numerical errors when the cos value of the joint angle is close to 1 ($\frac{d}{dx} \arccos x = -\frac{1}{\sqrt{1-x^2}}$). To deal with this issue, we derive an approximate upper bound for the changes of joint angle value to avoid computing the arccos function and its gradient. Again, take the right of Fig. 2 as an example, the angle change $\Delta\theta_9$ caused by the displacement of joint-9 (i.e., $x_9^{\tau'} - x_9^\tau$, $y_9^{\tau'} - y_9^\tau$, $z_9^{\tau'} - z_9^\tau$) can be approximated

by $\sin \Delta\theta_9 \approx \frac{\sqrt{(x_9^{\tau'} - x_9^\tau)^2 + (y_9^{\tau'} - y_9^\tau)^2 + (z_9^{\tau'} - z_9^\tau)^2}}{\sqrt{(x_{10}^\tau - x_9^\tau)^2 + (y_{10}^\tau - y_9^\tau)^2 + (z_{10}^\tau - z_9^\tau)^2}}$. In particular, when the angle change $\Delta\theta$ is smaller than 0.1 (i.e., 5.73°), we can consider $\sin \Delta\theta$ almost same as $\Delta\theta$. The total angle change $\Delta\theta$ is upper bounded by the sum of the changes caused by the displacements caused by joint-9, joint-10, and joint-11. Therefore the upper bound can be represented by $J^\tau = \frac{\sqrt{(x_9^{\tau'} - x_9^\tau)^2 + (y_9^{\tau'} - y_9^\tau)^2 + (z_9^{\tau'} - z_9^\tau)^2}}{\sqrt{(x_{10}^\tau - x_9^\tau)^2 + (y_{10}^\tau - y_9^\tau)^2 + (z_{10}^\tau - z_9^\tau)^2}} + \frac{\sqrt{(x_{10}^{\tau'} - x_{10}^\tau)^2 + (y_{10}^{\tau'} - y_{10}^\tau)^2 + (z_{10}^{\tau'} - z_{10}^\tau)^2}}{\sqrt{(x_{10}^\tau - x_9^\tau)^2 + (y_{10}^\tau - y_9^\tau)^2 + (z_{10}^\tau - z_9^\tau)^2}} + \frac{\sqrt{(x_{11}^{\tau'} - x_{11}^\tau)^2 + (y_{11}^{\tau'} - y_{11}^\tau)^2 + (z_{11}^{\tau'} - z_{11}^\tau)^2}}{\sqrt{(x_{11}^\tau - x_{10}^\tau)^2 + (y_{11}^\tau - y_{10}^\tau)^2 + (z_{11}^\tau - z_{10}^\tau)^2}}$. Although this representation looks more complicated than the arccos function, its gradient can be computed efficiently and accurately. Given such an approximation, the joint angle constraints can be similarly represented as

$$\max\{J_k^\tau - \epsilon_J, 0\} = 0 \quad (6)$$

where ϵ_J is set as $0.1 \sim 0.2$ ($6^\circ \sim 12^\circ$).

4.3 Speed Constraints

According to the physical conditions of human beings, we should consider one more type of constraints, i.e., temporal smoothness constraints. By those constraints, we attempt to restrict the speeds of the motions in the generated adversarial skeleton actions. Specifically, the speeds of the motions can be approximated by the displacements between two consecutive temporal frames, i.e., $S_m^\tau \approx \sqrt{(x_m^{\tau+1} - x_m^\tau)^2 + (y_m^{\tau+1} - y_m^\tau)^2 + (z_m^{\tau+1} - z_m^\tau)^2}$. Then, similar to Eq. 5, we bound the change of speeds by

$$\max\{|S_m^{\tau'} - S_m^\tau|/S_m^\tau - \epsilon_S, 0\} = 0, \quad (7)$$

where ϵ_L is usually set as (smaller than) 10%.

4.4 Constrained Primal Problem Formulation

In this subsection, we introduce the main objectives used under the untargeted setting and targeted setting.

Untargeted Setting. Under the untargeted setting, the adversary achieves its goal as long as the DNN makes a prediction other than the ground-truth label, i.e., $\arg\max_k F_{\Theta,k}(\mathbf{x}') \neq l$. This will hold

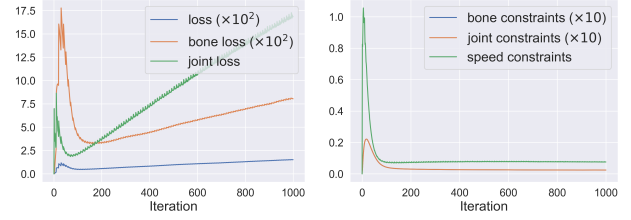


Figure 3: Evolution of the averaged loss items and the constraints ($\beta = 1.0$)

iff $F_{\Theta,l}(\mathbf{x}') < \max_{k,k \neq l} F_{\Theta,k}(\mathbf{x}')$. Therefore, we define the objective as minimizing $\max\{F_{\Theta,l}(\mathbf{x}') - \max_{k,k \neq l} F_{\Theta,k}(\mathbf{x}') + \text{conf}, 0\}$, where $\text{conf} > 0$ is the desired confidence value of the DNN on the wrong prediction. Note that if the objective is equal to 0, we have $\max_{k,k \neq l} F_{\Theta,k}(\mathbf{x}') \geq F_{\Theta,l}(\mathbf{x}') + \text{conf}$.

Targeted Setting. The goal of the adversary is to render the prediction result to be the attack target l_t , i.e., $\arg\max_{k \in \mathcal{K}} F_{\Theta,k}(\mathbf{x}') = l_t$. Therefore, the primal objective is defined as minimizing the cross entropy between $F_{\Theta,k}(\mathbf{x}')$ and l_t , or $\max\{\max_{k,k \neq l_t} F_{\Theta,k}(\mathbf{x}') - F_{\Theta,l_t}(\mathbf{x}') + \text{conf}, 0\}$ following the logic of the untargeted setting.

We can also adopt other objectives for our purpose. However, it turns out the above two main objectives are the most commonly-used ones in previous work [5, 16, 24]. For simplicity, we denote the main loss by $\mathcal{L}(\mathbf{x}, l)$. The constrained primal problem can then be formulated as

$$\min_{\mathbf{x}'} \mathcal{L}(\mathbf{x}', l) \quad (8)$$

subject to Eq. (5), (6), (7)

4.5 Dual Optimization by ADMM

Note that our constrained primal problems are in general intractable. Instead of searching for a solution to the constrained primal problem, we propose to formulate and optimize its unconstrained dual problem via ADMM. The algorithm is illustrated in Alg. 1. Specifically, we first define the augmented Lagrangian of the constrained primal as shown in Alg. 1. The additional term $\frac{\beta}{2}(\|\mathbf{B}'\|^2 + \|\mathbf{J}'\|^2 + \|\mathbf{S}'\|^2)$, which is commonly used in ADMM (for nonconvex problems), aims to further penalize any violation of the equality constraints. We note that larger β usually leads to smaller violation but larger final main objective (decreases the attack success rate).

Specifically, given the Lagrangian $\mathcal{G}(\mathbf{x}, l; \boldsymbol{\lambda}, \mathbf{v}, \boldsymbol{\omega})$ (defined in Alg. 1), the dual problem is $\max_{\boldsymbol{\lambda}, \mathbf{v}, \boldsymbol{\omega}} \min_{\mathbf{x}'} \mathcal{G}(\mathbf{x}, l; \boldsymbol{\lambda}, \mathbf{v}, \boldsymbol{\omega})$. Note that since the internal function $\min_{\mathbf{x}'} \mathcal{G}(\mathbf{x}, l; \boldsymbol{\lambda}, \mathbf{v}, \boldsymbol{\omega})$ is an affine function w.r.t. the variables $\boldsymbol{\lambda}, \mathbf{v}, \boldsymbol{\omega}$, we can simply use single-step gradient ascent with a large step size (usually set as β in ADMM) to update those dual variables. However, $\mathcal{G}(\mathbf{x}, l; \boldsymbol{\lambda}, \mathbf{v}, \boldsymbol{\omega})$ is an extremely complicated nonconvex function w.r.t. the adversarial sample \mathbf{x}' . Therefore, in most cases, we could only guarantee local optima for the internal minimization problem. Fortunately, it turns out that even the local optima can always fool the DNNs. To find a local optimum efficiently, we adopt the Adam optimizer instead of the vanilla stochastic gradient descent (SGD) since Adam optimizer always converges faster than vanilla SGD. Theoretically, a

local minimum is guaranteed because the Adam optimizer stops updating the variables when the gradients are (close to) 0. Next, we further look into the evolution of the loss during the optimization process. As shown in Fig. 3, at the very beginning (*i.e.*, the first stage), the internal minimization problem finds adversarial samples with large violation of the constraints. The large violation will cause the Lagrangian multipliers λ, ν, ω to increase rapidly, and thus significantly increase the loss terms $\langle \lambda, \mathbf{B}' \rangle$ (bone loss), $\langle \nu, \mathbf{J}' \rangle$ (joint loss), and $\langle \omega, \mathbf{S}' \rangle$ (speed loss). As a result, the algorithm proceeds into the second stage, where the Adam optimizer focuses more on diminishing the constraint violation \mathbf{B}', \mathbf{J}' , and \mathbf{S}' when optimizing \mathbf{x}' . Finally, the algorithm proceeds into a relatively stable stage where we can stop the algorithm. According to Fig. 2, our algorithm is very efficient in the sense that it only needs 200 (internal) iterations to enter the final stable stage.

Algorithm 1 Generating Adversarial Skeleton Actions

Require: Loss function $\mathcal{L}(\mathbf{x}, l)$, hyper-parameter β , adam optimizer for the adversarial skeleton action \mathbf{x}' , maximum number of iterations T .

Define Constraints: $\mathcal{B}_j^\tau \triangleq \max\{|B_j'^\tau - B_j^\tau|/B_j^\tau - \epsilon_L, 0\}$, $\mathcal{J}_k^\tau \triangleq \max\{|J_k'^\tau - \epsilon_J, 0\}$, and $\mathcal{S}_m^\tau \triangleq \max\{|S_m'^\tau - S_m^\tau|/S_m^\tau - \epsilon_S, 0\}$. (Vector Representations: \mathbf{B}', \mathbf{J}' , and \mathbf{S}')

Define Lagrangian Variables: λ, ν , and ω (Corresponding to \mathbf{B}', \mathbf{J}' , and \mathbf{S}')

Define Augmented Lagrangian: $\mathcal{G}(\mathbf{x}, l; \lambda, \nu, \omega) \triangleq \mathcal{L}(\mathbf{x}, l) + \langle \lambda, \mathbf{B}' \rangle + \langle \nu, \mathbf{J}' \rangle + \langle \omega, \mathbf{S}' \rangle + \frac{\beta}{2}(\|\mathbf{B}'\|^2 + \|\mathbf{J}'\|^2 + \|\mathbf{S}'\|^2)$.

for $t = 0$ to $T - 1$ **do**

Update \mathbf{x}' : fix the multipliers $\lambda(t), \nu(t), \omega(t)$

$\mathbf{x}'(t+1) \in \arg\min_{\mathbf{x}'} \mathcal{G}(\mathbf{x}', l; \lambda(t), \nu(t), \omega(t))$ updated by the adam optimizer

Update Multipliers: compute $\mathbf{B}'(t+1), \mathbf{J}'(t+1)$, and \mathbf{S}' based on \mathbf{x}'

$\lambda(t+1) = \lambda(t) + \beta \mathcal{B}'(t+1)$; $\nu(t+1) = \nu(t) + \beta \mathcal{J}'(t+1)$;
 $\omega(t+1) = \omega(t) + \beta \mathcal{S}'(t+1)$

end for

Output $\mathbf{x}'(T)$

5 DEFENSE AGAINST ADVERSARIAL SKELETON ACTIONS

Note that although the method proposed in [7, 19] can certify larger robust radii than [18]. However, the sample complexity to compute the confidence intervals in [7, 19] will lead to computational overhead in the inference stage. *Therefore, we only use the method in [7] in the certification process. In the inference stage, we modify the method in [18] to build a relatively efficient defense against adversarial skeleton actions, as shown in Alg. 2.* In general, our proposed defense consists of two steps: adding Gaussian noise and temporal filtering by Gaussian kernel. In the following, we will detail these two steps and explain why we include them in the defense.

5.1 Additive Gaussian Noise

Our first step is adding Gaussian noise to the skeleton actions. In the inference stage, we follow [18] to make the prediction as

$\arg\max_k E(\mathbf{F}_{\Theta, k}(\mathcal{M}(\mathbf{x}')))$ given input \mathbf{x}' , where $\mathcal{M}(\mathbf{x}) = \mathbf{G}(\mathbf{x} + \mathbf{z})$ is randomized mechanism with Gaussian noise \mathbf{z} and post-processing function \mathbf{G} . In order to estimate $E(\mathbf{F}_{\Theta}(\mathcal{M}(\mathbf{x}')))$, we sample N noisy samples $\tilde{\mathbf{x}}'(n) = \mathbf{x}' + \tilde{\mathbf{z}}(n)$ from $\mathcal{N}(\mathbf{x}', \sigma^2 \mathbf{I})$ and feed them into the post-processing function \mathbf{G} and the neural network \mathbf{F} . $E(\mathbf{F}_{\Theta}(\mathcal{M}(\mathbf{x}')))$ is estimated by $\frac{1}{N} \sum_{n=1}^N \mathbf{F}_{\Theta}(\mathbf{G}(\tilde{\mathbf{x}}'(n)))$, and according to the Chernoff bound [4], the error of this estimation is bounded by

$$Pr(|\frac{1}{N} \sum_{n=1}^N \mathbf{F}_{\Theta, l}(\mathbf{G}(\tilde{\mathbf{x}}'(n))) - E(\mathbf{F}_{\Theta, l}(\mathcal{M}(\mathbf{x}')))| < \epsilon) \sim \mathcal{O}(e^{-N\epsilon^2})$$

In the certification stage, we rely on the main theorem from [7], which gives the currently tightest bound:

LEMMA 1. Denote an mechanism randomized by Gaussian noise by $\mathcal{M}(\mathbf{x}) = \mathbf{G}(\mathbf{x} + \mathbf{z})$, and the ground-truth label by l . Define $f(\mathbf{x}) = \arg\max_k \mathbf{F}_{\Theta, k}(\mathcal{M}(\mathbf{x}))$. Suppose \underline{p}_A & \overline{p}_B satisfy

$$Pr(f(\mathbf{x}) = l) \geq \underline{p}_A \geq \overline{p}_B \geq \max_{i \neq l} Pr(f(\mathbf{x}) = i), \quad (9)$$

the ℓ_2 robust radius is $R = \frac{\sigma}{2}(\Phi^{-1}(\underline{p}_A) - \Phi^{-1}(\overline{p}_B))$.

Lemma 1 indicates that as long as $\|\mathbf{x}' - \mathbf{x}\|_2 < R$, $\arg\max_i Pr(f(\mathbf{x}) = i) = l$, *i.e.*, the prediction is correct. The algorithm using the above lemma for certification is detailed in Algorithm 3. In the next subsection, we will detail the post-processing function mentioned before.

Algorithm 2 Defense (Inference)

Require: Neural Network $\mathbf{F}_{\Theta}(\cdot)$, standard deviation of the additive Gaussian noise σ , skeleton action \mathbf{x}' (probably adversarial), number of noisy samples for inference of n .

Sample N samples from $\mathcal{N}(\mathbf{x}', \sigma^2 \mathbf{I}) \rightarrow \{\tilde{\mathbf{x}}'(n) | n = 1, 2, \dots, N\}$

Smooth $\tilde{\mathbf{x}}'(n)$ by a 1×5 or 1×7 Gaussian filter $\rightarrow \mathbf{G}(\tilde{\mathbf{x}}'(n))$

Feed $\mathbf{G}(\tilde{\mathbf{x}}'(n))$ into the network $\rightarrow \mathbf{F}_{\Theta}(\mathbf{G}(\tilde{\mathbf{x}}'(n)))$

Output $\arg\max_l \sum_{n=1}^N \mathbf{F}_{\Theta, l}(\mathbf{G}(\tilde{\mathbf{x}}'(n)))$

5.2 Temporal Filtering by Gaussian Kernel

After adding Gaussian noise to the skeleton actions, we propose to further smooths the action along the temporal axis by a 1×5 or 1×7 Gaussian filter. The intuition is that the adjacent frames in a skeleton action sequence are very similar to each other, and thus can be used as references to rectify the adversarial perturbations. Although this additional operation does not improve the certification results, we observe that it can help our defense become more compatible with a normally trained model than the original randomized smoothing method in [7, 18]. Also, we argue that this simple operation is not usually used in previous work because it is not very suitable in the image recognition domain, where no adjacency information (along the temporal axis) is available.

6 EXPERIMENTS

6.1 Attack Performance

Main Results. The main results of our attack are shown in Table 5. As we can see, our proposed attack can achieve 100% success

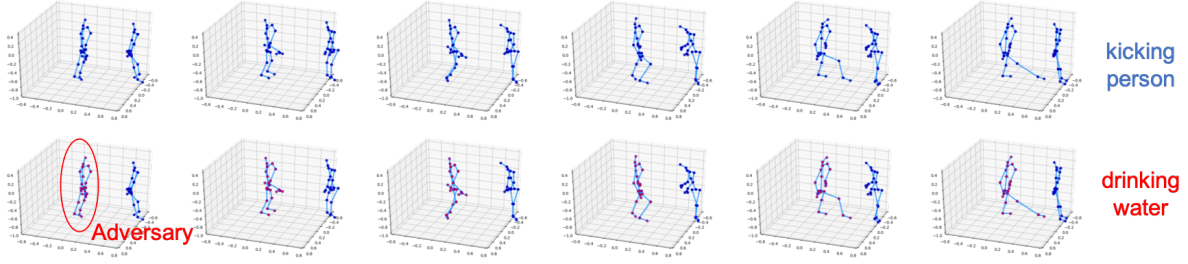


Figure 4: The top six frames represent a “kicking (another person)” skeleton action, and the bottom six frames are the corresponding frames from the adversarial skeleton action generated by our attack under the targeted setting (optimizing the first person). The generated adversarial skeleton action is recognized as “drinking water” by the 2s-AGCN.

White-box Untargeted	β	NTU CV					NTU CS				
		Success Rate	$\Delta B/B$	ΔJ	$\Delta K/K$	ℓ_2	Success Rate	$\Delta L/L$	ΔJ	$\Delta K/K$	ℓ_2
HCN	0.1	100%	2.64%	0.132	4.52%	0.396	100%	2.17%	0.111	3.17%	0.347
	1.0	100%	1.92%	0.099	1.65%	0.330	100%	1.62%	0.086	1.30%	0.290
	10.0	92.8%	1.50%	0.085	1.25%	0.270	92.4%	1.25%	0.073	0.98%	0.241
2s-AGCN	0.1	100%	2.17%	0.112	1.62%	0.653	100%	1.97%	0.107	2.20%	0.614
	1.0	100%	1.70%	0.094	0.59%	0.528	100%	1.46%	0.086	0.57%	0.496
	10.0	99.0%	1.37%	0.083	0.39%	0.428	98.8%	1.19%	0.078	0.34%	0.413
White-box targeted	β	NTU CV					NTU CS				
		Success Rate	$\Delta B/B$	ΔJ	$\Delta K/K$	ℓ_2	Success Rate	$\Delta L/L$	ΔJ	$\Delta K/K$	ℓ_2
HCN	0.1	100%	3.60%	0.165	7.75%	0.673	100%	3.55%	0.165	6.68%	0.723
	1.0	99.7%	3.24%	0.156	4.69%	0.630	100%	3.16%	0.155	4.24%	0.674
	10.0	22.3%	2.27%	0.115	2.83%	0.444	26.9%	2.14%	0.112	2.50%	0.462
2s-AGCN	0.1	100%	1.66%	0.090	0.55%	0.569	100%	1.67%	0.091	0.71%	0.649
	1.0	100%	1.61%	0.091	0.42%	0.556	100%	1.56%	0.090	0.49%	0.615
	10.0	97.2%	1.54%	0.089	0.38%	0.512	97.9%	1.47%	0.087	0.40%	0.552

Table 1: The *empirical* performance of our proposed method: averaged bone-length difference between original and adversarial skeletons ($\Delta L/L$), averaged joint angle difference (upper bound) ($\Delta J/J$), kinetic energy difference ($\Delta K/K$), ℓ_2 distance (ℓ_2).

Algorithm 3 Defense (Certification)

Require: Neural Network $F_\Theta(\cdot)$, standard deviation of the additive Gaussian noise σ , original and adversarial skeleton action \mathbf{x} & \mathbf{x}' , number of noisy samples for inference of n , a predefined confidence value p for hypothesis test (usually 95%).

Recognition: Sample N samples from $\mathcal{N}(\mathbf{x}, \sigma^2 \mathbf{I}) \rightarrow \{\tilde{\mathbf{x}}(n) | n = 1, 2, \dots, N\}$

Smooth $\tilde{\mathbf{x}}(n)$ by a 1×5 or 1×7 Gaussian filter $\rightarrow \mathbf{G}(\tilde{\mathbf{x}}(n))$

Feed $\tilde{\mathbf{x}}(n)$ into the (normally trained) network $\rightarrow F_\Theta(\mathbf{G}(\tilde{\mathbf{x}}(n)))$

Confidence Interval: Compute the number (counts) top two indices in $\{\arg\max_k F_{\Theta,k}(\mathbf{G}(\tilde{\mathbf{x}}(n))) | n = 1, 2, \dots, N\} \rightarrow c_A, c_B$
Compute the lower bound for p_A and the upper bound for p_B by the method in [11] with confidence $p \rightarrow p_A, \overline{p_B}$.

Certification: Compute the certified ℓ_2 radius by $R = \frac{\sigma}{2}(\Phi^{-1}(p_A) - \Phi^{-1}(\overline{p_B}))$.

Output $\max\{R, 0\}$ if p_A corresponds to the ground-truth label l else -1

Compare R with $\|\mathbf{x}' - \mathbf{x}\|_2$, and if R is larger, then output the index corresponding to c_A .

rates with very small violation of the constraints. The averaged normalized bone-length difference is approximately 1% ~ 2%, and the violation of the joint angles is smaller than 10° . *Considering the skeleton data is usually noisy, this subtle violation is considered “very common” in real world.* We also provide more experimental results in the supplementary material (e.g., on Kinetics).

We also note that adversarial-sample generation under the untargeted setting is usually easier than that under the targeted setting since a targeted adversarial sample is guaranteed to be an untargeted adversarial sample, but not vice versa. This fact is also reflected by the results in Table 5. Furthermore, in Figure 4, we show the visualization result of an adversarial skeleton action (recognized as a normal action “drinking water”) generated by our attack, which is almost visually indistinguishable from its original skeleton action (“kicking”). Figures of more adversarial actions are attached in the appendix.

Transferability. In order to shed light on the transferability of our attack, we feed the adversarial skeleton actions generated on a HCN model to another HCN model and 2s-AGCN, respectively. In order to boost the transferability performance, we set β as 0.01 or 0.1 to generate adversarial skeleton actions with larger perturbation. The attack success rates are given in Table 2. *Similar to 3D adversarial*

Source (Model) → Target	Dataset	$\beta = 0.1$	$\beta = 0.01$
HCN(1) → HCN(2)	NTU CV	24.7%	26.0%
	NTU CS	28.5%	32.6%
HCN(1) → 2s-AGCN	NTU CV	17.6%	20.4%
	NTU CS	17.3%	19.6%

Table 2: Attack success rates of adversarial examples transferred between models.

Untargeted	Success Rate	$\Delta B/B$	ΔJ	$\Delta K/K$	ℓ_2
NTU CV	100%	4.67%	0.241	13.0%	0.278
NTU CS	100%	4.09%	0.211	10.2%	0.244
Targeted	Success Rate	$\Delta B/B$	ΔJ	$\Delta K/K$	ℓ_2
NTU CV	100%	8.82%	0.468	38.1%	0.510
NTU CS	100%	9.45%	0.507	36.8%	0.520

Table 3: Adversarial skeleton actions generated by C&W attack on HCN (ℓ_2 distance is smaller).

Model	Setting	NTU CV		NTU CS	
		$\sigma = 0.01$	$\sigma = 0.02$	$\sigma = 0.01$	$\sigma = 0.02$
HCN	Untargeted	62.0%	62.3%	50.6%	51.4%
	Targeted	79.4%	70.8%	67.1%	58.3%
2s-AGCN	Untargeted	51.0%	42.2%	42.1%	40.2%
	Targeted	60.8%	50.5%	42.2%	44.1%

Table 4: Empirical performance (model accuracy) of our proposed defense on normally trained model.

point clouds [36], the transferability of the adversarial skeleton actions is also a little limited compared with adversarial images.

Comparison with C&W Attack. We use C&W attack as an example to shed light on the difference between our attack and the existing attacks. C&W attack has been demonstrated as a successful optimization-based adversarial attack in many application domains. However, since C&W attack mainly considers minimizing the ℓ_2 distance between original and adversarial skeletons, it might easily violate the constraints, as shown in our simple case study (Table 3).

6.2 Defense Performance

Empirical Results. We demonstrate the performance of the defense for inference in Table 4. We set $\beta = 1.0$ to generate adversarial examples, and set $N = 50$ (Alg. 2), which is more smaller than the number of samples required for certification but can achieve good empirical performance, as shown in Table 4. *it is much easier to defend adversarial skeleton actions under the targeted setting than the untargeted setting.* Note that the accuracy of HCN on NTU-CV and NTU-CS is respectively 91.1% and 86.5% [20], and the accuracy of 2s-AGCN is respectively 95.1% and 88.5% [29].

Certified Results. Due to the high computational cost of the certification method ($N=1000$), we mainly evaluate the certification algorithm on HCN. The certified accuracy achieved by different levels of noise is shown in Fig. 5. Note that we use the same level of noise to train the model as the noise for certification. As we can

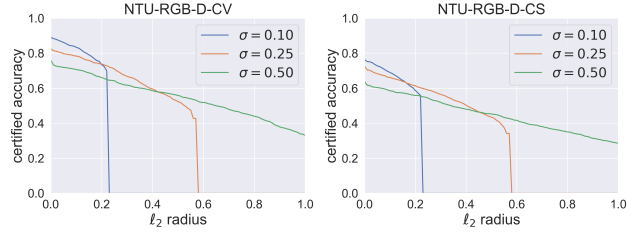


Figure 5: Certification accuracy on HCN

see, with sacrificing 10% ~ 20% accuracy on the clean samples, the method is able to achieve about 50% certified accuracy ($\ell_2 = 0.5$).

7 CONCLUSION

We study the problem of adversarial vulnerability of skeleton-based action recognition. We first identify and formulate three main constraints that should be considered in adversarial skeleton actions. Since the corresponding constrained optimization problem is intractable, we propose to optimize its dual problem by ADMM, which is a generic method first proposed in this paper to generate constrained adversarial examples. To defend against adversarial skeleton actions, we further specify an efficient defensive inference algorithm and a certification algorithm. The effectiveness of the attack and defense is demonstrated on two opensource models, and the results induce several interesting observations that can help us understand more about adversarial skeleton actions.

REFERENCES

- [1] Maksym Andriushchenko, Francesco Croce, Nicolas Flammarion, and Matthias Hein. 2019. Square Attack: a query-efficient black-box adversarial attack via random search. *arXiv preprint arXiv:1912.00049* (2019).
- [2] Anish Athalye, Nicholas Carlini, and David Wagner. 2018. Obfuscated gradients give a false sense of security: Circumventing defenses to adversarial examples. *arXiv preprint arXiv:1802.00420* (2018).
- [3] José M Bioucas-Dias and Mário AT Figueiredo. 2010. Alternating direction algorithms for constrained sparse regression: Application to hyperspectral unmixing. In *2010 2nd Workshop on Hyperspectral Image and Signal Processing: Evolution in Remote Sensing*. IEEE, 1–4.
- [4] Stéphane Boucheron, Gábor Lugosi, and Pascal Massart. 2013. *Concentration inequalities: A nonasymptotic theory of independence*. Oxford university press.
- [5] Nicholas Carlini and David Wagner. 2017. Towards evaluating the robustness of neural networks. In *Security and Privacy (SP), 2017 IEEE Symposium on*. IEEE, 39–57.
- [6] Guangchun Cheng, Yiwen Wan, Abdullah N Saudagar, Kamesh Namuduri, and Bill P Buckles. 2015. Advances in human action recognition: A survey. *arXiv preprint arXiv:1501.05964* (2015).
- [7] Jeremy M Cohen, Elan Rosenfeld, and J Zico Kolter. 2019. Certified adversarial robustness via randomized smoothing. *arXiv preprint arXiv:1902.02918* (2019).
- [8] Krishnamurthy Dvijotham, Robert Stanforth, Sven Gowal, Timothy A Mann, and Pushmeet Kohli. 2018. A Dual Approach to Scalable Verification of Deep Networks.. In *UAI*. 550–559.
- [9] Pedro A Forero, Alfonso Cano, and Georgios B Giannakis. 2010. Consensus-based distributed support vector machines. *Journal of Machine Learning Research* 11, May (2010), 1663–1707.
- [10] Ian J Goodfellow, Jonathon Shlens, and Christian Szegedy. 2014. Explaining and harnessing adversarial examples. *arXiv preprint arXiv:1412.6572* (2014).
- [11] Leo A Goodman. 1965. On simultaneous confidence intervals for multinomial proportions. *Technometrics* 7, 2 (1965), 247–254.
- [12] Sven Gowal, Krishnamurthy Dvijotham, Robert Stanforth, Rudy Bunel, Chongli Qin, Jonathan Uesato, Timothy Mann, and Pushmeet Kohli. 2018. On the effectiveness of interval bound propagation for training verifiably robust models. *arXiv preprint arXiv:1810.12715* (2018).
- [13] Warren He, James Wei, Xinyun Chen, Nicholas Carlini, and Dawn Song. 2017. Adversarial example defense: Ensembles of weak defenses are not strong. In *11th USENIX Workshop on Offensive Technologies (WOOT 17)*.

- [14] Jinyuan Jia, Xiaoyu Cao, Binghui Wang, and Neil Zhenqiang Gong. 2019. Certified Robustness for Top-k Predictions against Adversarial Perturbations via Randomized Smoothing. *arXiv preprint arXiv:1912.09899* (2019).
- [15] Qihong Ke, Mohammed Bennamoun, Senjian An, Ferdous Sohel, and Farid Bousaid. 2017. A new representation of skeleton sequences for 3d action recognition. In *Proceedings of the IEEE conference on computer vision and pattern recognition*. 3288–3297.
- [16] Alexey Kurakin, Ian Goodfellow, and Samy Bengio. 2016. Adversarial machine learning at scale. *arXiv preprint arXiv:1611.01236* (2016).
- [17] Rongjie Lai and Stanley Osher. 2014. A splitting method for orthogonality constrained problems. *Journal of Scientific Computing* 58, 2 (2014), 431–449.
- [18] Mathias Lecuyer, Vaggelis Atlidakis, Roxana Geambasu, Daniel Hsu, and Suman Jana. 2018. Certified robustness to adversarial examples with differential privacy. *arXiv preprint arXiv:1802.03471* (2018).
- [19] Bai Li, Changyou Chen, Wenlin Wang, and Lawrence Carin. 2018. Second-order adversarial attack and certifiable robustness. *arXiv preprint arXiv:1809.03113* (2018).
- [20] Chao Li, Qiaoyong Zhong, Di Xie, and Shiliang Pu. 2018. Co-occurrence feature learning from skeleton data for action recognition and detection with hierarchical aggregation. *arXiv preprint arXiv:1804.06055* (2018).
- [21] Shuai Li, Wanqing Li, Chris Cook, Ce Zhu, and Yanbo Gao. 2018. Independently Recurrent Neural Network (IndRNN): Building a Longer and Deeper RNN. In *The IEEE Conference on Computer Vision and Pattern Recognition (CVPR)*.
- [22] Jian Liu, Naveed Akhtar, and Ajmal Mian. 2019. Adversarial Attack on Skeleton-based Human Action Recognition. *arXiv preprint arXiv:1909.06500* (2019).
- [23] Ziyu Liu, Hongwen Zhang, Zhenghao Chen, Zhiyong Wang, and Wanli Ouyang. 2020. Disentangling and Unifying Graph Convolutions for Skeleton-Based Action Recognition. *arXiv preprint arXiv:2003.14111* (2020).
- [24] Aleksander Madry, Aleksandar Makelov, Ludwig Schmidt, Dimitris Tsipras, and Adrian Vladu. 2017. Towards deep learning models resistant to adversarial attacks. *arXiv preprint arXiv:1706.06083* (2017).
- [25] Ondrej Miksik, Vibhav Vineet, Patrick Pérez, Philip HS Torr, and F Cesson Sévigné. 2014. Distributed non-convex admm-inference in large-scale random fields. In *British Machine Vision Conference (BMVC)*, Vol. 2.
- [26] Matthew Mirman, Timon Gehr, and Martin Vechev. 2018. Differentiable abstract interpretation for provably robust neural networks. In *International Conference on Machine Learning*. 3575–3583.
- [27] Aditi Raghunathan, Jacob Steinhardt, and Percy Liang. 2018. Certified defenses against adversarial examples. *arXiv preprint arXiv:1801.09344* (2018).
- [28] Amir Shahroudy, Jun Liu, Tian-Tsong Ng, and Gang Wang. 2016. NTU RGB+D: A large scale dataset for 3D human activity analysis. In *Proceedings of the IEEE conference on computer vision and pattern recognition*. 1010–1019.
- [29] Lei Shi, Yifan Zhang, Jian Cheng, and Hanqing Lu. 2019. Two-stream adaptive graph convolutional networks for skeleton-based action recognition. In *Proceedings of the IEEE Conference on Computer Vision and Pattern Recognition*. 12026–12035.
- [30] Chenyang Si, Wentao Chen, Wei Wang, Liang Wang, and Tieniu Tan. 2019. An attention enhanced graph convolutional lstm network for skeleton-based action recognition. In *Proceedings of the IEEE Conference on Computer Vision and Pattern Recognition*. 1227–1236.
- [31] Yusuke Tashiro, Yang Song, and Stefano Ermon. 2020. Output Diversified Initialization for Adversarial Attacks. *arXiv preprint arXiv:2003.06878* (2020).
- [32] Jonathan Uesato, Brendan O’Donoghue, Pushmeet Kohli, and Aaron Oord. 2018. Adversarial Risk and the Dangers of Evaluating Against Weak Attacks. In *International Conference on Machine Learning*. 5032–5041.
- [33] Shiqi Wang, Kexin Pei, Justin Whitehouse, Junfeng Yang, and Suman Jana. 2018. Efficient formal safety analysis of neural networks. In *Advances in Neural Information Processing Systems*. 6367–6377.
- [34] Yu Wang, Wotao Yin, and Jinshan Zeng. 2019. Global convergence of ADMM in nonconvex nonsmooth optimization. *Journal of Scientific Computing* 78, 1 (2019), 29–63.
- [35] Eric Wong and Zico Kolter. 2018. Provable defenses against adversarial examples via the convex outer adversarial polytope. In *International Conference on Machine Learning*. 5283–5292.
- [36] Chong Xiang, Charles R Qi, and Bo Li. 2018. Generating 3d adversarial point clouds. *arXiv preprint arXiv:1809.07016* (2018).
- [37] Sijie Yan, Yuanjun Xiong, and Dahua Lin. 2018. Spatial temporal graph convolutional networks for skeleton-based action recognition. In *Thirty-Second AAAI Conference on Artificial Intelligence*.
- [38] Allen Y Yang, Zihan Zhou, Arvind Ganesh Balasubramanian, S Shankar Sastry, and Yi Ma. 2013. Fast ℓ_1 -Minimization Algorithms for Robust Face Recognition. *IEEE Transactions on Image Processing* 22, 8 (2013), 3234–3246.
- [39] Hongyang Zhang, Yaodong Yu, Jiantao Jiao, Eric P Xing, Laurent El Ghaoui, and Michael I Jordan. 2019. Theoretically principled trade-off between robustness and accuracy. *arXiv preprint arXiv:1901.08573* (2019).
- [40] Pu Zhao, Sijia Liu, Yanzhi Wang, and Xue Lin. 2018. An admm-based universal framework for adversarial attacks on deep neural networks. In *Proceedings of the 26th ACM international conference on Multimedia*. 1065–1073.
- [41] Tianhang Zheng, Changyou Chen, and Kui Ren. 2019. Distributionally adversarial attack. In *Proceedings of the AAAI Conference on Artificial Intelligence*, Vol. 33. 2253–2260.

A APPENDIX

Additional visualization results. Here we provide more visualization results. We use “drinking water” as the attack target because “drinking water” is a normal action, which looks completely different from the some violent/abnormal actions like throwing, kicking, pushing, and punching. Despite the obvious visual difference between “drinking water” and those abnormal actions, our attack can still fool the state-of-the-art models to recognize those abnormal actions as “drinking water” by imperceptible and reproducible perturbation, which indicates that our attack is very powerful. In Fig. 6, we show that our attack can fool the HCN model to recognize the “throwing”, “pushing”, and “kicking” actions as a normal action “drinking water” by imperceptible adversarial perturbation. Similarly, in Fig. 7, we show that our attack can fool the 2s-AGCN model to recognize the “throwing” and “pushing” actions as a normal action “drinking water”. These visualization results along with the quantitative results in Table 1 (in the paper) demonstrate that the perturbations are indeed imperceptible and reproducible.

Kinetics Dataset. Except for the NTU dataset, we also evaluate our attack on another popular dataset, *i.e.*, Kinetics-400 dataset under both the untargeted and targeted settings. As shown in Table 5, under the untargeted setting, our attack can achieve 100% attack success rates with very small violation of the constraints, similar to its performance on the NTU dataset. However, under the targeted setting, it is much more difficult for our attack to find targeted adversarial skeleton actions with very small violation of the constraints. This is because Kinetics-400 has 400 classes of actions, and the original NTU dataset only has 60 classes of actions. Also, we argue that the results on Kinetics under the targeted setting do not devalue our attack since even for most of the clean testing samples from Kinetics, it is difficult for the state-of-the-models to predict their ground-truth labels (targets).

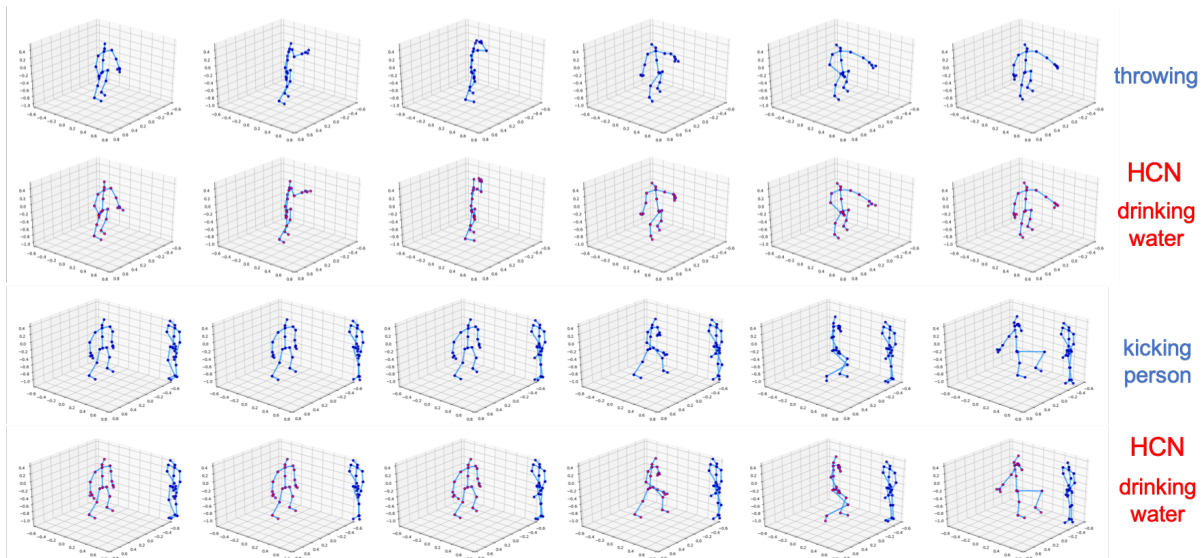


Figure 6: The adversarial skeleton actions generated by our attack under the targeted setting. The generated adversarial skeleton actions are recognized as “drinking water” by the HCN.

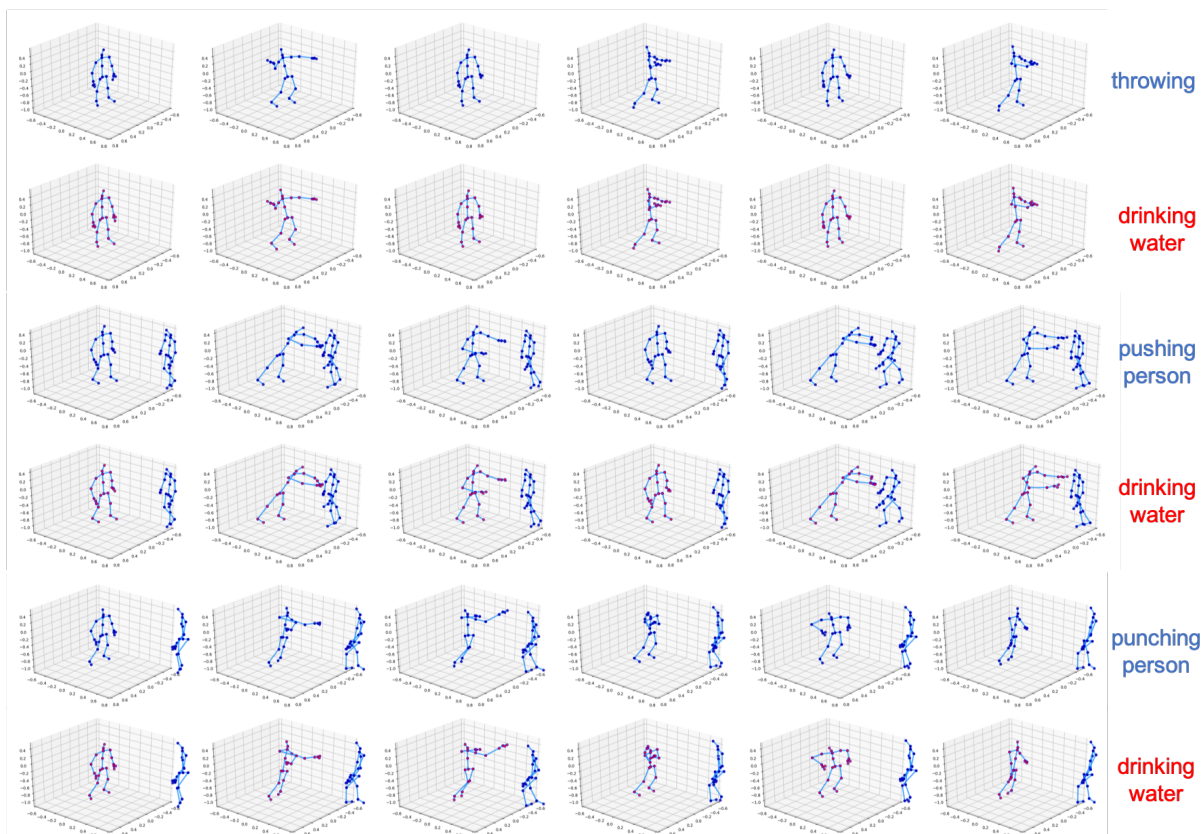


Figure 7: The adversarial skeleton actions generated by our attack under the targeted setting. The generated adversarial skeleton action is recognized as “drinking water” by the 2s-AGCN.

Untargeted	β	Kinetics-400				
		Success Rate	$\Delta B/B$	ΔJ	$\Delta K/K$	ℓ_2
HCN	0.1	100%	2.60%	0.082	1.66%	0.150
	1.0	100%	2.58%	0.080	1.52%	0.162
	10.0	98.8%	2.49%	0.078	1.21%	0.145
2s-AGCN	0.1	100%	0.91%	0.053	0.58%	0.331
	1.0	100%	0.77%	0.047	0.53%	0.298
	10.0	100%	0.75%	0.046	0.52%	0.287
Targeted	β	Kinetics-400				
		Success Rate	$\Delta B/B$	ΔJ	$\Delta K/K$	ℓ_2
HCN	0.1	90.2%	5.22%	0.220	11.2%	1.864
	1.0	67.2%	2.79%	0.124	4.86%	1.350
	10.0	17.2%	1.44%	0.073	2.36%	0.763
2s-AGCN	0.1	99.2%	5.25%	0.167	1.20%	0.725
	1.0	98.8%	5.04%	0.159	1.21%	0.722
	10.0	98.4%	4.89%	0.153	1.03%	0.677

Table 5: The performance of our proposed attack on Kinetics: success rate, averaged bone-length difference between original and adversarial skeletons ($\Delta L/L$), averaged joint angle difference (upper bound) ($\Delta J/J$), kinetic energy difference ($\Delta K/K$), ℓ_2 distance (ℓ_2).